Scientific Reports

https://doi.org/10.1038/s41598-026-40762-6

Article in Press

Integrated transcriptomic analysis of the temporal cortex identifies CRH and GAD2 as neuropathological markers and reveals altered immune microenvironment in Alzheimer's disease

Received: 23 December 2025

Accepted: 16 February 2026

Published online: 25 February 2026

Cite this article as: Liu P., Huang C., Lu L. *et al.* Integrated transcriptomic analysis of the temporal cortex identifies CRH and GAD2 as neuropathological markers and reveals altered immune microenvironment in Alzheimer's disease. *Sci Rep* (2026). https://doi.org/10.1038/s41598-026-40762-6

Pan Liu, ChengLong Huang, Lin Lu, Yi Lin Pang & ZhaoYang Huang

Integrated Transcriptomic Analysis of the Temporal Cortex Identifies CRH and GAD2 as Neuropathological Markers and Reveals Altered Immune Microenvironment in Alzheimer's Disease

Pan Liu[1,*], ChengLong Huang [1,*], Lin Lu[2], Yi Lin Pang[3,#], ZhaoYang Huang[1,#]

[1] Department of Clinical Laboratory, Renmin Hospital of Wuhan University, Wuhan, China,

[2] Department of Orthopedics, Renmin Hospital of Wuhan University, Wuhan, China,

[3] College of Bioscience and Biotechnology, Hunan Agricultural University, Changsha, Hunan, China.

Corresponding author: **ZhaoYang Huang**, Wuhan 430060, Hubei, China. and **Yi Lin Pang**, Changsha, Hunan, 410128, China.
Email address: huangzhy85@mail2.sysu.edu.cn or ylpang2010@126.com
*These authors made equal contributions to this work.

Abstract

Background: Alzheimer's disease (AD) is a progressive neurodegenerative disorder characterized by complex neuroimmune interactions. Identifying reliable neuropathological markers and understanding immune cell infiltration in the brain are essential for improving our understanding of AD pathology.
Methods: We integrated four temporal cortex gene expression datasets from the GEO database (GSE36980, GSE37263, GSE118553, GSE122063). Differentially expressed genes (DEGs) were identified using RobustRankAggreg (RRA) and batch correction. Functional enrichment was analyzed via GO and KEGG, and hub genes were identified through protein-protein interaction networks and comparative intersection analysis. Diagnostic performance was evaluated using ROC curves, and immune cell infiltration was profiled with CIBERSORT, with significant immune subsets identified via Wilcoxon tests and LASSO regression.
Results: Analysis revealed 98 robust DEGs, prominently enriched in pathways related to synaptic transmission and neuroactive ligand-receptor interactions. Two hub genes, CRH and GAD2, were identified and validated as being significantly downregulated in AD. ROC analysis affirmed their high discriminatory value (AUC $\geq$ 0.7), with a combined model demonstrating good performance. Immune infiltration profiling in the AD temporal cortex uncovered significant alterations in six immune cell populations: M2 macrophages, activated dendritic cells, and resting mast cells were increased,

while plasma cells, regulatory T cells (Tregs), and activated NK cells were decreased. However, no significant correlation was found between the expression of CRH/GAD2 and these immune cell alterations.
Conclusion: CRH and GAD2 are potential neuropathological markers for AD. The distinct immune infiltration patterns observed highlight the involvement of both innate and adaptive immunity in AD pathogenesis, offering new insights for understanding AD pathology and informing future therapeutic strategies. The lack of direct correlation suggests that neuronal gene dysregulation and immune alterations may represent parallel or independently regulated pathological dimensions in AD.

Keywords Alzheimer disease, Diagnostic biomarkers, Immune cell infiltration, Bioinformatics, CRH, GAD2

Introduction

First described by Alois Alzheimer in 1907 [1], Alzheimer's disease (AD) is a progressive neurodegenerative disorder and the predominant cause of dementia among middle-aged and older adults [2]. Its pathological hallmarks include the accumulation of cerebral amyloid-β plaques and neurofibrillary tau tangles, which drive synaptic dysfunction, neuronal loss, and the progression of cognitive decline [3]. In the United States alone, AD affects an estimated 6.9 million individuals aged 65 and older, a figure projected to double by 2060 [4]. The gold-standard neuropathological diagnosis of AD relies on assessing the distribution and burden of these brain pathologies [5]. Despite its prevalence and significant impact, achieving a definitive diagnosis of AD prior to death remains a considerable challenge.

Chronic immune activation is recognized as a pivotal factor in AD pathogenesis [6]. Neuroinflammation, which can be triggered by factors such as infection, brain injury, stress, or aging, involves the activation of brain-resident cells like microglia and astrocytes [7]. Sustained inflammation leads to the release of proinflammatory molecules, resulting in synaptic damage, neurodegeneration, and cognitive deficits [8]. Growing evidence indicates that the infiltration of peripheral immune cells and their crosstalk with central nervous system-resident cells contribute to AD pathology [9]. For instance, Chen et al. [10] demonstrated that microglia-induced T cell infiltration accelerates neurodegeneration in models of tauopathy. Lu et al. [11] proposed that peripheral natural killer (NK) cells may infiltrate the brain and influence Alzheimer's-related neuroinflammation, with STAT3 potentially modulating immunity-related genes in these cells. Furthermore, Jorfi et al. [9] found that $CD8^+$ T cells exacerbate AD pathology in a 3D human neuroimmune axis model. These insights highlight the critical need for continued investigation into immune cell infiltration and its connection to diagnostic biomarkers to deepen our understanding and improve the diagnosis of AD.

To this end, the present study analyzed four GEO datasets (GSE36980, GSE37263, GSE118553, and GSE122063) to identify differentially expressed

genes (DEGs) between AD and healthy control (HC) samples from the temporal cortex. The functional implications of these genes were evaluated through Gene Ontology (GO) and Kyoto Encyclopedia of Genes and Genomes (KEGG) pathway analyses. Hub genes were identified using the 'UpSet' R package, and the diagnostic potential of candidate biomarkers was assessed via Receiver Operating Characteristic (ROC) curve analysis combined with logistic regression. Furthermore, immune cell infiltration in AD was examined using CIBERSORT, with Wilcoxon tests and LASSO regression applied to identify significantly altered immune cell subsets. Associations between the identified biomarkers and immune cell changes were explored using Spearman's rank correlation analysis. This research provides a systematic assessment of immune cell infiltration in the AD temporal cortex, identifies potential neuropathological markers, and offers new insights for developing pathomechanistic and therapeutic strategies.

Materials and methods

Data Acquisition

The analytical workflow for this study is depicted in Fig. 1. Gene expression profiles from the temporal cortex of AD patients and HCs were retrieved from five initial datasets (GSE36980, GSE37263, GSE118553, GSE122063, and GSE132903) available in the GEO database. Detailed information regarding the microarray platforms, sample groups, sample sizes, and available demographic details (age, sex) for each dataset is provided in Table 1 and Supplementary Table S1.

Data Preprocessing and Integration

For the four microarray datasets (GSE36980, GSE37263, GSE118553, GSE122063), probe-level expression data were background-corrected and normalized using the Robust Multiarray Average (RMA) algorithm implemented in the 'affy' R package. Probes were subsequently annotated to genes using the respective platform annotation files, and expression values for genes mapped by multiple probes were averaged. The normalized gene expression matrices from the four datasets were merged using a Perl script. To mitigate technical batch effects and platform heterogeneity, the 'sva' R package was employed. The integrated and batch-corrected gene expression matrix was then subjected to subsequent analysis using the 'limma' R package. The validation dataset GSE132903, an RNA-Seq dataset, was processed and analyzed using the 'edgeR' package. Data quality and intra-group sample reproducibility were assessed using Principal Component Analysis (PCA), Pearson's correlation analysis, and sample clustering, with results visualized via the 'ggplot2' package.

Identification of DEGs

DEGs between AD and HC groups were identified using two complementary approaches to ensure robustness. In the "Batch Correction" method, the four integrated and batch-corrected datasets were analyzed as a single matrix

using the 'limma' package. In the "RobustRankAggreg (RRA)" method, each dataset was analyzed independently for DEGs using 'limma', and the resulting gene lists were aggregated using the 'RobustRankAggreg' package, which assigns a significance score based on the rank order of genes across multiple studies. The final consensus set of robust DEGs was determined by intersecting the results from both methods, applying a significance threshold of an adjusted *p*-value < 0.05 and an absolute log2 fold change > 0.585 (corresponding to an approximate 1.5-fold change).

Functional enrichment analysis

The biological functions and pathways associated with the identified DEGs were investigated through GO and KEGG enrichment analyses. These analyses were performed using the 'ClusterProfiler' R package (v4.6.2) with annotations from the 'org.Hs.eg.db' database (v3.16.0). Enrichment was performed for all genes in the background list. The minimum gene set size was set to 10 and the maximum to 500. Terms with an adjusted p-value < 0.05 were considered statistically significant. The results were visualized using the 'enrichplot' and 'ggplot2' packages.

Hub Gene Identification and Validation

A protein–protein interaction (PPI) network was constructed for the protein-coding DEGs using the STRING database, with a high-confidence minimum interaction score set to 0.9. The resulting network file was imported into Cytoscape (v3.9.1). The cytoHubba plugin was utilized to rank nodes within the network using ten different algorithms (e.g., MCC, DMNC, Betweenness). The top 40 genes from each algorithm were analyzed using the 'UpSet' R package (v1.4.0) to perform a comparative intersection analysis to identify the most frequently occurring hub genes across all methods. The expression patterns of these candidate hub genes were subsequently validated using the independent RNA-Seq dataset GSE132903.

Evaluation of Diagnostic Potential

The diagnostic performance of the validated hub genes was assessed using Receiver Operating Characteristic (ROC) curve analysis. The Area Under the Curve (AUC) was calculated for each gene individually and for a combined logistic regression model to evaluate their ability to discriminate between AD patients and HCs in the GSE132903 validation dataset. The predictive accuracy of the combined model was further quantified using a confusion matrix.

Experimental Validation via RT-qPCR

To biologically validate the bioinformatic findings, temporal cortex samples were obtained postmortem, comprising six HCs and ten confirmed AD cases (in the dementia stage) collected between May 2025 and August 2025. Detailed demographic and sample information (age, sex, post-mortem interval) for this cohort is provided in Supplementary Table S2. Total RNA was extracted using TRIzol reagent (Thermo Fisher Scientific), and cDNA was synthesized with the HiScript IV RT SuperMix kit (Vazyme Biotech).

Quantitative real-time PCR (RT-qPCR) was performed using ChamQ Universal SYBR qPCR Master Mix (Vazyme Biotech) on a Bio-Rad iQ5 system. The thermal cycling protocol consisted of an initial denaturation at 94°C for 5 min, followed by 40 cycles of 94°C for 15 s and 60°C for 30 s. Gene expression was normalized to GAPDH, and relative quantification was determined using the $2^{-\Delta\Delta CT}$ method using the average ΔCT value of the healthy control group as the calibrator. Primer sequences are listed in Table 2.

Analysis of Immune Cell Infiltration

The relative abundances of 22 human immune cell subtypes within the temporal cortex samples were estimated using the CIBERSORT algorithm and its LM22 signature matrix [12]. Only samples with a CIBERSORT output *p*-value < 0.05 were included for subsequent analysis, resulting in 178 high-quality samples. The 'Cibersort' R package was used to generate immune cell proportion estimates, visualized via bar plots and correlation heatmaps. Differential immune cell infiltration between AD and HC groups was identified using the Wilcoxon rank-sum test. To refine the selection of the most discriminative immune cell subsets, a Least Absolute Shrinkage and Selection Operator (LASSO) regression analysis was performed using the 'glmnet' package. Immune cell types identified as significant by both the Wilcoxon test ($p < 0.05$) and LASSO regression were considered the final set of differentially infiltrated cells. The relationship between the expression levels of the hub genes and the proportions of these key immune cells was examined using Spearman's rank correlation analysis and visualized with 'ggplot2'.

Statistical analysis

All statistical analyses, unless otherwise specified, were conducted using R software (version 4.2.3). For the bioinformatic analyses using public datasets where full covariates were not uniformly available, comparisons were performed between AD and HC groups without adjustment for demographic variables. Data from RT-qPCR are expressed as mean ± standard error of the mean (SEM). Group comparisons for RT-qPCR data were performed using an unpaired Student's *t*-test. The ages and PMI between the AD and HC groups in our validation cohort were compared using *t*-tests and showed no statistically significant difference ($p > 0.05$; see Supplementary Table S2). For correlation analyses involving hub genes and immune cells, Spearman's method was used. A *p*-value of less than 0.05 was considered statistically significant for all tests.

Results

Differential Gene Expression Analysis

DEGs were identified from four microarray datasets, encompassing 98 AD and 80 normal control samples, using two distinct methodological approaches. Supplementary Figure S1 demonstrates the efficacy of the batch correction process, with panels A-B showing the merged dataset prior to correction and panels C-D confirming the successful removal of batch effects. Application of

the RRA method yielded 143 DEGs (40 upregulated, 103 downregulated), a subset of which is displayed in Fig. 2A. Concurrently, the "Batch correction" method identified 130 DEGs (35 upregulated, 95 downregulated). The expression profile of these DEGs is visualized in a heatmap (Fig. 2B). Intersection of the DEGs from both methods produced a robust, consensus set of 98 DEGs, comprising 23 upregulated and 75 downregulated genes, as illustrated in the Venn diagram (Fig. 2C).

Functional Enrichment of DEGs

The 98 overlapping DEGs were subjected to GO and KEGG pathway enrichment analyses to elucidate their biological significance (Fig. 3A-D). GO analysis revealed significant enrichment in terms related to synaptic signaling and neurological processes, including "modulation of chemical synaptic transmission," "regulation of trans-synaptic signaling," "signal release," "learning or memory," "hormone transport," and "cognition" (Fig. 3A-B). KEGG pathway analysis indicated that the DEGs were predominantly involved in "Neuroactive ligand-receptor interaction," "GABAergic synapse," "Retrograde endocannabinoid signaling," "Morphine addiction," "Apelin signaling pathway," "Alcoholism," and "Nicotine addiction" (Fig. 3C-D).

Identification and Validation of Hub Genes

A PPI network was constructed from the 98 overlapping DEGs. The network nodes were subsequently ranked using ten different algorithms within the cytoHubba plugin. Cross-analysis of the top-ranked genes from all algorithms using a comparative intersection analysis identified two central hub genes: *CRH* and *GAD2*, which are highlighted in Fig. 4A. Their expression patterns within the merged microarray dataset are further illustrated via a heatmap (Fig. 4B) and a volcano plot (Fig. 4C). To validate these findings, the independent RNA-Seq dataset GSE132903 was analyzed, which confirmed a significant downregulation of both *CRH* and *GAD2* in AD temporal cortex samples compared to healthy controls ($p < 0.001$; Fig. 5A-C). This decreased mRNA expression was further corroborated experimentally using RT-qPCR on postmortem temporal cortex samples (Fig. 6A-B and Supplementary Table S3).

Diagnostic Efficacy of Hub Genes

The diagnostic potential of CRH and GAD2 as biomarkers for AD was evaluated using ROC curve analysis on the GSE132903 dataset. As shown in Fig. 5D, both genes individually demonstrated considerable discriminatory power, with AUC values ≥ 0.7. A logistic regression model integrating both hub genes was subsequently developed, demonstrating good diagnostic efficacy with a specificity of 0.66, a sensitivity of 0.76, and an AUC of 0.749 ($p = 9.372e{-}10$), surpassing the performance of each gene individually (Fig. 5E-F). For comparative purposes, the predictive performance of 27 previously reported AD biomarker genes from the literature was assessed [13-17]. ROC analysis revealed that only 7 of these genes (*ADCYAP1*, *ATP6V1D*, *CAP2*, *VIP*, *PPP3R1*, *DDIT4*, and *NDUFA1*) achieved an AUC > 0.7 (Fig. 7). Notably, when combined into a single diagnostic model, these literature-derived genes yielded a higher

combined AUC value than the two-gene model from this study, with the AUC increasing as more genes were added to the model.

Immune Cell Infiltration Landscape in the Temporal Cortex

CIBERSORT analysis was performed on 178 quality-filtered samples (98 AD, 80 HC; $p < 0.05$) to characterize the immune cell infiltration profile. The relative proportions of 22 immune cell types in each sample are depicted in a histogram (Fig. 8A) and a heatmap (Fig. 8B). The predominant infiltrating immune cell populations included M1 macrophages, activated memory $CD4^+$ T cells, resting NK cells, activated dendritic cells, and M2 macrophages (Fig. 8B). Correlation analysis among the 22 immune cell types in AD tissues (Fig. 8C) revealed several significant relationships, including a positive correlation between activated NK cells and follicular helper T cells, a positive association between neutrophils and M2 macrophages, a negative correlation between M2 and M0 macrophages, and an inverse relationship between resting and activated NK cells.

To rigorously identify differentially infiltrated immune cells, the results from a Wilcoxon rank-sum test (Fig. 9A) and LASSO regression analysis (Fig. 9B-C) using the lambda.1se value for final variable selection were integrated. The intersection of these two methods identified six immune cell types with consistent and significant alterations in AD (Fig. 10A). Specifically, AD temporal cortex tissues exhibited significantly elevated infiltration of M2 macrophages, activated dendritic cells, and resting mast cells, alongside significantly reduced proportions of plasma cells, regulatory T cells (Tregs), and activated NK cells compared to healthy controls (Fig. 9A).

Correlation Between Hub Genes and Immune Cells

The potential relationships between the two hub genes (*CRH*, *GAD2*) and the six significantly altered immune cell types were investigated using Spearman's correlation analysis. The results of these analyses are summarized in Fig. 10B. Applying a stringent threshold ($R > 0.40$ and $p < 0.001$), no statistically significant correlations were identified between the expression levels of either CRH or GAD2 and the infiltration levels of any of the six immune cell types.

Discussion

The accurate and early diagnosis of AD dementia is critical for effective intervention, yet it remains a significant clinical challenge. While established biomarkers from cerebrospinal fluid (CSF) [18] and positron emission tomography (PET) [19] have been available for decades, their widespread clinical adoption is hindered by issues of accessibility, cost, perceived invasiveness, and the historical lack of disease-modifying therapies [20]. Consequently, recent research has intensified its focus on identifying minimally invasive biomarkers in blood (e.g., phosphorylated Tau) [21], genetic risk factors (e.g., APOE) [22-24], and other body fluids [25]. However, the translation of these discoveries into routine clinical practice remains limited. This underscores an urgent need to identify highly sensitive and specific genetic signatures and to validate them in clinical specimens to

provide new options for understanding AD pathology and identifying potential therapeutic targets.

This study consolidated gene expression data specifically from the temporal cortex, a region severely affected by AD pathology. Our functional enrichment analysis of the 98 robust DEGs indicates that AD is fundamentally characterized by a disruption of neurological homeostasis, manifesting as multidimensional impairments in synaptic transmission, neural signaling, and cognitive function (Fig. 3). This conclusion is corroborated by other transcriptomic investigations. For example, Jin et al. [13] similarly reported that disrupted nervous system homeostasis is a central feature of AD, based on enrichment analysis of overlapping hub genes identified in their study. Furthermore, analyses of frontal cortical samples by Zhang et al. [26] underscored the significant involvement of immune response and oxidative stress pathways, reinforcing the concept that AD pathogenesis involves a complex interplay of multiple biological processes beyond synaptic dysfunction.

Through a rigorous bioinformatics workflow employing a comparative intersection analysis and ROC analysis, we identified CRH and GAD2 as potential neuropathological markers for AD. A combined diagnostic model utilizing both genes demonstrated good efficacy compared to single-gene models. The significant downregulation of both *CRH* and *GAD2* in the AD temporal cortex was subsequently validated using an independent RNA-Seq dataset and confirmed experimentally via RT-qPCR. The direction of change (downregulation) was consistent across microarray and RNA-seq technologies, supporting the robustness of this finding. Corticotropin-releasing hormone (CRH), a key regulator of the HPA (hypothalamic-pituitary-adrenal) axis [27], is involved in stress response [28, 29] and possesses neuroprotective properties against oxidative and excitotoxic stress [30]. Its role, however, extends to immunomodulation, acting through both anti-inflammatory (central) and pro-inflammatory (peripheral) pathways [31]. Our finding of CRH downregulation in AD temporal cortex aligns with reports of reduced CRH levels in the CSF of AD patients [32], suggesting a disruption in stress response systems and neuroprotective mechanisms. The GAD2 gene, encoding the GAD65 enzyme crucial for GABA synthesis, has been implicated in various conditions, from obesity [33] to psychiatric disorders [34]. Its restricted tissue expression has also made it a diagnostic marker for certain tumors [35]. Importantly, GAD2 has been previously linked to AD. Studies have proposed it as a drug target [36, 37], and robust evidence from multiple groups [38, 39] has consistently demonstrated reduced GAD2 levels in several AD-affected brain regions, including the temporal cortex. This collective evidence strongly supports the role of CRH and GAD2 dysregulation in AD and underscores their potential as neuropathological markers and therapeutic targets.

Our findings contribute to a growing body of literature employing bioinformatics to identify AD-related gene signatures. Other studies have

identified hub genes related to vascular dementia [40], autophagy [41], and mitophagy [42], or core DEGs like SCG3 [43], achieving varying degrees of diagnostic accuracy (AUCs). In a comparative analysis of published gene signatures [13-17], we observed that diagnostic models incorporating more genes generally yield higher performance. While the individual discriminatory power of CRH and GAD2 was notable, this suggests that future efforts should focus on integrating them with other high-performing, literature-derived genes to develop an optimized multi-gene diagnostic panel for AD, validated in larger cohorts. Their value lies in highlighting specific dysregulated pathways (e.g., neuroactive ligand-receptor interaction, GABAergic synapse) that are central to AD pathology in the temporal cortex, rather than as standalone superior diagnostic tools.

Beyond gene signatures, this study provides a systematic characterization of the immune cell infiltration landscape in the AD temporal cortex. CIBERSORT analysis revealed a profoundly altered immune microenvironment. The convergence of Wilcoxon test and LASSO regression results pinpointed six key altered immune subsets: increased M2 macrophages, activated dendritic cells, and resting mast cells, alongside decreased plasma cells, regulatory T cells (Tregs), and activated NK cells.

The elevation of M2 macrophages and activated dendritic cells is consistent with a state of chronic neuroinflammation. It is important to note that the CIBERSORT analysis, based on a peripheral blood-derived signature matrix, cannot definitively distinguish between infiltrating peripheral macrophages and resident microglia. The observed "M2 macrophage" signature likely represents a mixture of these cell types, primarily reflecting an activated, potentially disease-associated microglial state. While M2 macrophages are often associated with tissue repair, their persistent activation in AD may contribute to pathology, for instance, by failing to effectively clear amyloid-beta or by secreting factors that disrupt neural homeostasis [44, 45]. Activated dendritic cells can initiate adaptive immune responses [46], and their presence suggests a bridge between innate and adaptive immunity in AD, potentially facilitating T-cell mediated neurodegeneration [47]. The reduction in Tregs, which are vital for maintaining immune tolerance, could lead to unchecked neuroinflammatory responses [48]. The decrease in activated NK cells points to a broader immune dysregulation, though their precise role in AD—whether neurotoxic or regulatory—remains to be fully elucidated [11].

Our immune findings both align with and refine the existing understanding of neuroinflammation in AD. The increases in M2 macrophages and decreases in plasma cells and activated NK cells are consistent with reports in other brain regions like the prefrontal cortex [13]. However, discrepancies, such as the status of Tregs and dendritic cells, highlight the regional heterogeneity of the neuroimmune response in AD [16]. Therefore, our study provides a crucial, region-specific immune profile of the vulnerable temporal cortex.

Notably, our correlation analysis did not reveal strong direct associations

between CRH/GAD2 expression and the levels of the six altered immune cell types. This suggests that the neuronal gene dysregulation and immune cell infiltration, while co-occurring in AD, may represent parallel pathological processes or interact through complex, non-linear mechanisms not captured by bulk-tissue correlation analysis. The effects of CRH on neuroinflammation are likely indirect, mediated systemically via the HPA axis [27, 31], while GAD2's role is primarily linked to GABAergic neurotransmission and neuronal resilience [49]. This absence of correlation is an important finding, indicating that these two key aspects of AD pathology might be regulated independently or through indirect, system-level interactions, warranting further investigation at single-cell resolution.

Limitations

Our study has several limitations. First, the identified markers CRH and GAD2 are downregulated, which can pose challenges for detection compared to upregulated markers; however, our validation across technologies supports the robustness of this finding. Second, the primary analysis utilized public datasets with incomplete demographic matching. While we validated findings in a local cohort matched for age and PMI, future studies with larger, prospectively collected cohorts are needed. Third, the CIBERSORT tool has inherent limitations in the brain context, as discussed, and the immune profiles should be interpreted as reflecting overall immune microenvironment changes rather than precise quantification of specific infiltrating peripheral cells. Finally, the sample size for our RT-qPCR validation, though sufficient to show statistical significance, is relatively small.

Conclusion

In summary, this integrated bioinformatics and experimental study identifies CRH and GAD2 as robust neuropathological markers for AD, characterized by significant downregulation and high discriminatory value in the temporal cortex. Furthermore, we delineate a comprehensive immune infiltration landscape in AD, revealing profound dysregulation of both innate and adaptive immune cells, including M2 macrophages, dendritic cells, mast cells, plasma cells, Tregs, and NK cells. The absence of a strong direct correlation between the biomarkers and specific immune cells suggests these are key, yet potentially independent, dimensions of AD pathology. Collectively, our findings provide novel candidate markers for understanding AD pathology and deepen the understanding of neuroimmune dysfunction in AD, thereby informing the future development of pathomechanistic and therapeutic strategies.

Abbreviations

AD	Alzheimer's disease
RRA	RobustRankAggreg
Tregs	regulatory T cells

NK	natural killer
GO	Gene Ontology
KEGG	Kyoto Encyclopedia of Genes and Genomes
ROC	Receiver Operating Characteristic
RMA	Robust Multiarray Average
PPI	protein–protein interaction
AUC	The area under the ROC curve
Ct	The threshold cycle
SEM	standard error of the mean
CSF	cerebrospinal fluid
PET	positron emission tomography
CRH	Corticotropin-releasing hormone
DLPFC	dorsolateral prefrontal cortex
BWS	Bu-Wang San

Supplementary Information

Supplementary material is accessible in the online version.
Supplementary Material 1
Supplementary Material 2
Supplementary Material 3

Acknowledgements

We extend our profound gratitude to the patients, their families, and caregivers for their invaluable participation and trust in this study.

Author contributions

Pan Liu and Chenglong Huang contributed equally as co-first authors. Their contributions included: conceptualization and study design, data collection, software utilization and formal analysis, methodology implementation and validation, and writing – original draft preparation.
Lin Lu contributions included:, data collection and software utilization.
Zhaoyang Huang and Yilin Pang contributed equally as co-corresponding authors. Their contributions included: supervision and project administration, funding acquisition, resource provision, writing – review and editing, and final approval of the version to be published.
All authors have read and approved the final manuscript and take full responsibility for the integrity and accuracy of all aspects of the work.

Funding

This work was supported by the National Natural Science Foundation of China (grant 82302026).

Data availability

The gene expression datasets used in this study are publicly available from the GEO database (accession numbers: GSE36980, GSE37263, GSE118553,

GSE122063, and GSE132903). The code supporting the findings is available at: https://github.com/caoyezi/analysis-code. Processed data are available from the corresponding author upon reasonable request.

Declarations

Ethics approval and consent to participate

The Institutional Review Board of the Institutional Ethics Committee at Renmin Hospital of Wuhan University, granted approval for this study (approval No.2025K-K290). The research was conducted in compliance with the principles outlined in the Declaration of Helsinki. Informed consent for participation in this study was obtained from the next of kin or legal guardians of the postmortem tissue donors.

Consent for publication

Not applicable.

Competing interests

The authors declare no competing interests.

References

1. Bhole RP, Chikhale RV, Rathi KM. Current biomarkers and treatment strategies in Alzheimer disease: An overview and future perspectives. IBRO neuroscience reports. 2024;16:8-42; doi: 10.1016/j.ibneur.2023.11.003.
2. McDade EM. Alzheimer Disease. Continuum (Minneapolis, Minn). 2022;28 3:648-75; doi: 10.1212/con.0000000000001131.
3. Day GS. Diagnosing Alzheimer Disease. Continuum (Minneapolis, Minn). 2024;30 6:1584-613; doi: 10.1212/con.0000000000001507.
4. Jaqua EE, Tran MN, Hanna M. Alzheimer Disease: Treatment of Cognitive and Functional Symptoms. American family physician. 2024;110 3:281-93.
5. Therriault J, Schindler SE, Salvadó G, Pascoal TA, Benedet AL, Ashton NJ, et al. Biomarker-based staging of Alzheimer disease: rationale and clinical applications. Nature reviews Neurology. 2024;20 4:232-44; doi: 10.1038/s41582-024-00942-2.
6. Mary A, Mancuso R, Heneka MT. Immune Activation in Alzheimer Disease. Annual review of immunology. 2024;42 1:585-613; doi: 10.1146/annurev-immunol-101921-035222.
7. Heneka MT, Carson MJ, El Khoury J, Landreth GE, Brosseron F, Feinstein DL, et al. Neuroinflammation in Alzheimer's disease. The Lancet Neurology. 2015;14 4:388-405; doi: 10.1016/s1474-4422(15)70016-5.
8. Kinney JW, Bemiller SM, Murtishaw AS, Leisgang AM, Salazar AM, Lamb BT. Inflammation as a central mechanism in Alzheimer's disease. Alzheimer's & dementia (New York, N Y). 2018;4:575-90; doi: 10.1016/j.trci.2018.06.014.
9. Jorfi M, Park J, Hall CK, Lin CJ, Chen M, von Maydell D, et al. Infiltrating CD8(+) T cells exacerbate Alzheimer's disease pathology in a 3D human

neuroimmune axis model. Nature neuroscience. 2023;26 9:1489-504; doi: 10.1038/s41593-023-01415-3.

10. Chen X, Firulyova M, Manis M, Herz J, Smirnov I, Aladyeva E, et al. Microglia-mediated T cell infiltration drives neurodegeneration in tauopathy. Nature. 2023;615 7953:668-77; doi: 10.1038/s41586-023-05788-0.
11. Lu Y, Li K, Hu Y, Wang X. Expression of Immune Related Genes and Possible Regulatory Mechanisms in Alzheimer's Disease. Frontiers in immunology. 2021;12:768966; doi: 10.3389/fimmu.2021.768966.
12. Newman AM, Steen CB, Liu CL, Gentles AJ, Chaudhuri AA, Scherer F, et al. Determining cell type abundance and expression from bulk tissues with digital cytometry. Nature biotechnology. 2019;37 7:773-82; doi: 10.1038/s41587-019-0114-2.
13. Jin F, Xi Y, Xie D, Wang Q. Comprehensive analysis reveals a 5-gene signature and immune cell infiltration in Alzheimer's disease with qPCR validation. Frontiers in genetics. 2022;13:913535; doi: 10.3389/fgene.2022.913535.
14. Lai Y, Lin P, Lin F, Chen M, Lin C, Lin X, et al. Identification of immune microenvironment subtypes and signature genes for Alzheimer's disease diagnosis and risk prediction based on explainable machine learning. Frontiers in immunology. 2022;13:1046410; doi: 10.3389/fimmu.2022.1046410.
15. Zhuang X, Zhang G, Bao M, Jiang G, Wang H, Li S, et al. Development of a novel immune infiltration-related diagnostic model for Alzheimer's disease using bioinformatic strategies. Frontiers in immunology. 2023;14:1147501; doi: 10.3389/fimmu.2023.1147501.
16. Tian Y, Lu Y, Cao Y, Dang C, Wang N, Tian K, et al. Identification of diagnostic signatures associated with immune infiltration in Alzheimer's disease by integrating bioinformatic analysis and machine-learning strategies. Frontiers in aging neuroscience. 2022;14:919614; doi: 10.3389/fnagi.2022.919614.
17. Duan K, Ma Y, Tan J, Miao Y, Zhang Q. Identification of genetic molecular markers and immune infiltration characteristics of Alzheimer's disease through weighted gene co-expression network analysis. Frontiers in neurology. 2022;13:947781; doi: 10.3389/fneur.2022.947781.
18. Vogelgsang J, Wiltfang J. [New biomarkers for Alzheimer's disease in cerebrospinal fluid and blood]. Der Nervenarzt. 2019;90 9:907-13; doi: 10.1007/s00115-019-0772-9.
19. Wang Y, Liao W, Wang L, Li J, Huang D, Cheng W, et al. Advance and Prospect of Positron Emission Tomography in Alzheimer's disease research. Molecular psychiatry. 2025;30 10:4899-909; doi: 10.1038/s41380-025-03081-2.
20. Assfaw AD, Schindler SE, Morris JC. Advances in blood biomarkers for Alzheimer disease (AD): A review. The Kaohsiung journal of medical

sciences. 2024;40 8:692-8; doi: 10.1002/kjm2.12870.

21. Thijssen EH, La Joie R, Strom A, Fonseca C, Iaccarino L, Wolf A, et al. Plasma phosphorylated tau 217 and phosphorylated tau 181 as biomarkers in Alzheimer's disease and frontotemporal lobar degeneration: a retrospective diagnostic performance study. The Lancet Neurology. 2021;20 9:739-52; doi: 10.1016/s1474-4422(21)00214-3.
22. Stevenson-Hoare J, Heslegrave A, Leonenko G, Fathalla D, Bellou E, Luckcuck L, et al. Plasma biomarkers and genetics in the diagnosis and prediction of Alzheimer's disease. Brain : a journal of neurology. 2023;146 2:690-9; doi: 10.1093/brain/awac128.
23. Koutsodendris N, Nelson MR, Rao A, Huang Y. Apolipoprotein E and Alzheimer's Disease: Findings, Hypotheses, and Potential Mechanisms. Annual review of pathology. 2022;17:73-99; doi: 10.1146/annurev-pathmechdis-030421-112756.
24. Deming Y, Vasiljevic E, Morrow A, Miao J, Van Hulle C, Jonaitis E, et al. Neuropathology-based APOE genetic risk score better quantifies Alzheimer's risk. Alzheimer's & dementia : the journal of the Alzheimer's Association. 2023;19 8:3406-16; doi: 10.1002/alz.12990.
25. Rajendran K, Krishnan UM. Biomarkers in Alzheimer's disease. Clinica chimica acta; international journal of clinical chemistry. 2024;562:119857; doi: 10.1016/j.cca.2024.119857.
26. Jin B, Cheng X, Fei G, Sang S, Zhong C. Identification of diagnostic biomarkers in Alzheimer's disease by integrated bioinformatic analysis and machine learning strategies. Frontiers in aging neuroscience. 2023;15:1169620; doi: 10.3389/fnagi.2023.1169620.
27. Swaab DF, Bao AM, Lucassen PJ. The stress system in the human brain in depression and neurodegeneration. Ageing research reviews. 2005;4 2:141-94; doi: 10.1016/j.arr.2005.03.003.
28. Chrousos GP, Zoumakis E. Milestones in CRH Research. Current molecular pharmacology. 2017;10 4:259-63; doi: 10.2174/1874467210666170109165219.
29. Zhang Y, Li X, Lu S, Guo H, Zhang Z, Zheng H, et al. Stress triggers gut dysbiosis via CRH-CRHR1-mitochondria pathway. NPJ biofilms and microbiomes. 2024;10 1:93; doi: 10.1038/s41522-024-00571-z.
30. Pedersen WA, McCullers D, Culmsee C, Haughey NJ, Herman JP, Mattson MP. Corticotropin-releasing hormone protects neurons against insults relevant to the pathogenesis of Alzheimer's disease. Neurobiology of disease. 2001;8 3:492-503; doi: 10.1006/nbdi.2001.0395.
31. Karalis K, Muglia LJ, Bae D, Hilderbrand H, Majzoub JA. CRH and the immune system. Journal of neuroimmunology. 1997;72 2:131-6; doi: 10.1016/s0165-5728(96)00178-6.
32. May C, Rapoport SI, Tomai TP, Chrousos GP, Gold PW. Cerebrospinal fluid concentrations of corticotropin-releasing hormone (CRH) and corticotropin (ACTH) are reduced in patients with Alzheimer's disease. Neurology.

1987;37 3:535-8; doi: 10.1212/wnl.37.3.535.

33. Tiwari HK, Bouchard L, Pérusse L, Allison DB. Is GAD2 on chromosome 10p12 a potential candidate gene for morbid obesity? Nutrition reviews. 2005;63 9:315-9; doi: 10.1111/j.1753-4887.2005.tb00147.x.
34. Davis KN, Tao R, Li C, Gao Y, Gondré-Lewis MC, Lipska BK, et al. GAD2 Alternative Transcripts in the Human Prefrontal Cortex, and in Schizophrenia and Affective Disorders. PloS one. 2016;11 2:e0148558; doi: 10.1371/journal.pone.0148558.
35. Lennartz M, Benjamin Dünnebier N, Höflmayer D, Dwertmann Rico S, Kind S, Reiswich V, et al. GAD2 Is a Highly Specific Marker for Neuroendocrine Neoplasms of the Pancreas. The American journal of surgical pathology. 2024;48 4:377-86; doi: 10.1097/pas.0000000000002186.
36. Mosharaf MP, Alam K, Gow J, Mahumud RA, Mollah MNH. Common molecular and pathophysiological underpinnings of delirium and Alzheimer's disease: molecular signatures and therapeutic indications. BMC geriatrics. 2024;24 1:716; doi: 10.1186/s12877-024-05289-3.
37. Wang H, Chao L, Shen S, You P, Li L, Chen X, et al. Exploring the pharmacological mechanism of Bu-Wang San on Alzheimer's disease through multiple GEO datasets of the human hippocampus, network pharmacology, and metabolomics based on GC-MS and UPLC-Q/TOF-MS. Journal of ethnopharmacology. 2025;350:119994; doi: 10.1016/j.jep.2025.119994.
38. Schwab C, Yu S, Wong W, McGeer EG, McGeer PL. GAD65, GAD67, and GABAT immunostaining in human brain and apparent GAD65 loss in Alzheimer's disease. Journal of Alzheimer's disease : JAD. 2013;33 4:1073-88; doi: 10.3233/jad-2012-121330.
39. Burbaeva G, Boksha IS, Tereshkina EB, Starodubtseva LI, Savushkina OK, Vorob'eva EA, et al. [A role of glutamate decarboxylase in Alzheimer's disease]. Zhurnal nevrologii i psikhiatrii imeni SS Korsakova. 2014;114 4:68-72.
40. Tian X, Qin Y, Tian Y, Ge X, Cui J, Han H, et al. Identification of vascular dementia and Alzheimer's disease hub genes expressed in the frontal lobe and temporal cortex by weighted co-expression network analysis and construction of a protein-protein interaction. The International journal of neuroscience. 2022;132 10:1049-60; doi: 10.1080/00207454.2020.1860966.
41. Xu W, Su X, Qin J, Jin Y, Zhang N, Huang S. Identification of Autophagy-Related Biomarkers and Diagnostic Model in Alzheimer's Disease. Genes. 2024;15 8; doi: 10.3390/genes15081027.
42. Liu J, Yan M, Chen L, Yu W, Lü Y. Construction and evaluation of a diagnostic model for Alzheimer's disease based on mitophagy-related genes. Scientific reports. 2025;15 1:10632; doi: 10.1038/s41598-025-89980-4.
43. Fan Y, Wang X, Ling Y, Wang Q, Zhou X, Li K, et al. Identification and validation of biomarkers in Alzheimer's disease based on machine learning

algorithms and single-cell sequencing analysis. Computational biology and chemistry. 2025;118:108475; doi: 10.1016/j.compbiolchem.2025.108475.

44. Darwish SF, Elbadry AMM, Elbokhomy AS, Salama GA, Salama RM. The dual face of microglia (M1/M2) as a potential target in the protective effect of nutraceuticals against neurodegenerative diseases. Frontiers in aging. 2023;4:1231706; doi: 10.3389/fragi.2023.1231706.
45. Sackmann V, Ansell A, Sackmann C, Lund H, Harris RA, Hallbeck M, et al. Anti-inflammatory (M2) macrophage media reduce transmission of oligomeric amyloid beta in differentiated SH-SY5Y cells. Neurobiology of aging. 2017;60:173-82; doi: 10.1016/j.neurobiolaging.2017.08.022.
46. Théry C, Amigorena S. The cell biology of antigen presentation in dendritic cells. Current opinion in immunology. 2001;13 1:45-51; doi: 10.1016/s0952-7915(00)00180-1.
47. Brezovakova V, Valachova B, Hanes J, Novak M, Jadhav S. Dendritic Cells as an Alternate Approach for Treatment of Neurodegenerative Disorders. Cellular and molecular neurobiology. 2018;38 6:1207-14; doi: 10.1007/s10571-018-0598-1.
48. Yang H, Park SY, Baek H, Lee C, Chung G, Liu X, et al. Adoptive therapy with amyloid-β specific regulatory T cells alleviates Alzheimer's disease. Theranostics. 2022;12 18:7668-80; doi: 10.7150/thno.75965.
49. Patel AB, de Graaf RA, Martin DL, Battaglioli G, Behar KL. Evidence that GAD65 mediates increased GABA synthesis during intense neuronal activity in vivo. Journal of neurochemistry. 2006;97 2:385-96; doi: 10.1111/j.1471-4159.2006.03741.x.

Figures

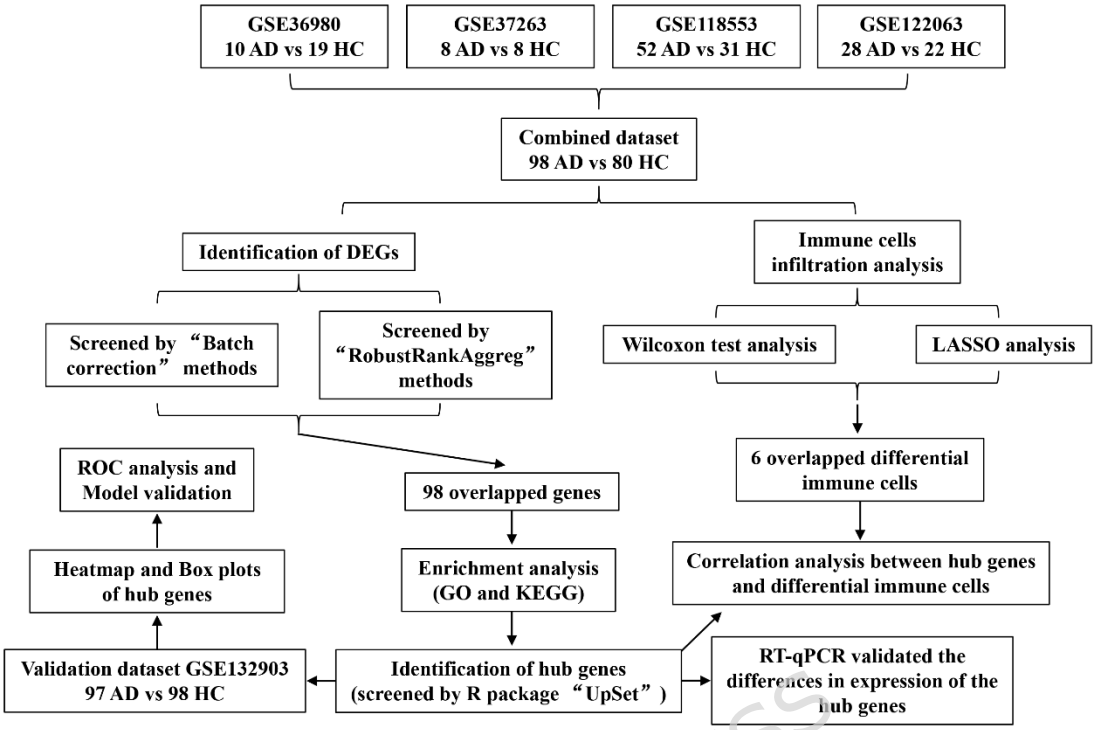

Fig. 1 Study flow chart.

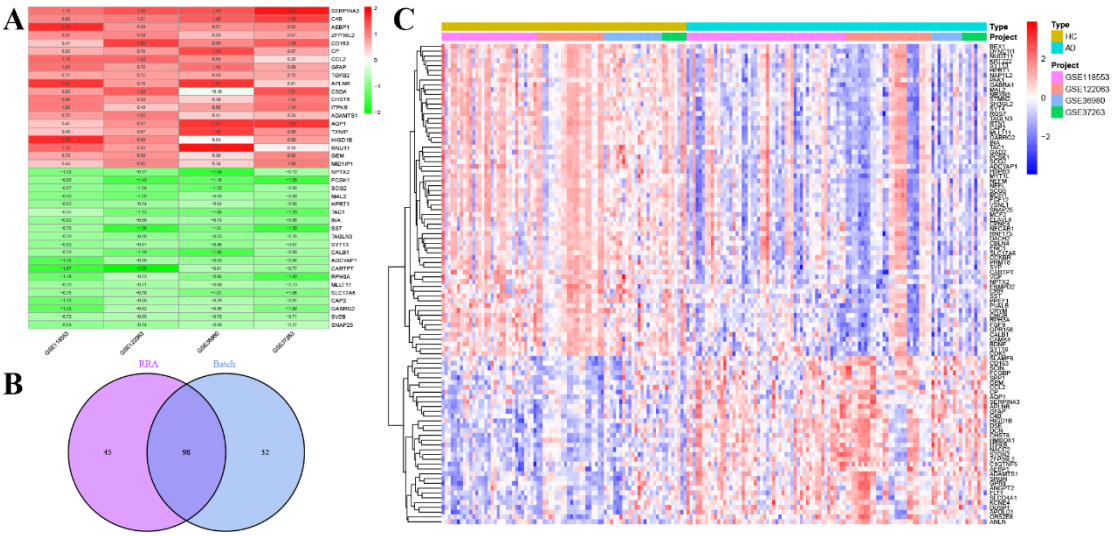

Fig. 2 Identification of DEGs. **(A)** The initial 40 upregulated and downregulated DEGs from the four datasets were identified using the 'RRA' method. Columns represent genes, rows represent samples (AD vs. HC), and the color scale from green to red indicates low to high expression (log2 normalized intensity). **(B)** Heatmap was used to depict the ultimate DEGs discovered by the "Batch correction" methods. Columns represent DEGs, rows represent samples. The color scale (see legend) indicates the Z-score of gene expression across samples, with red representing high expression and blue representing low expression. **(C)** A Venn diagram was used to identify the intersecting DEGs identified by both methods.

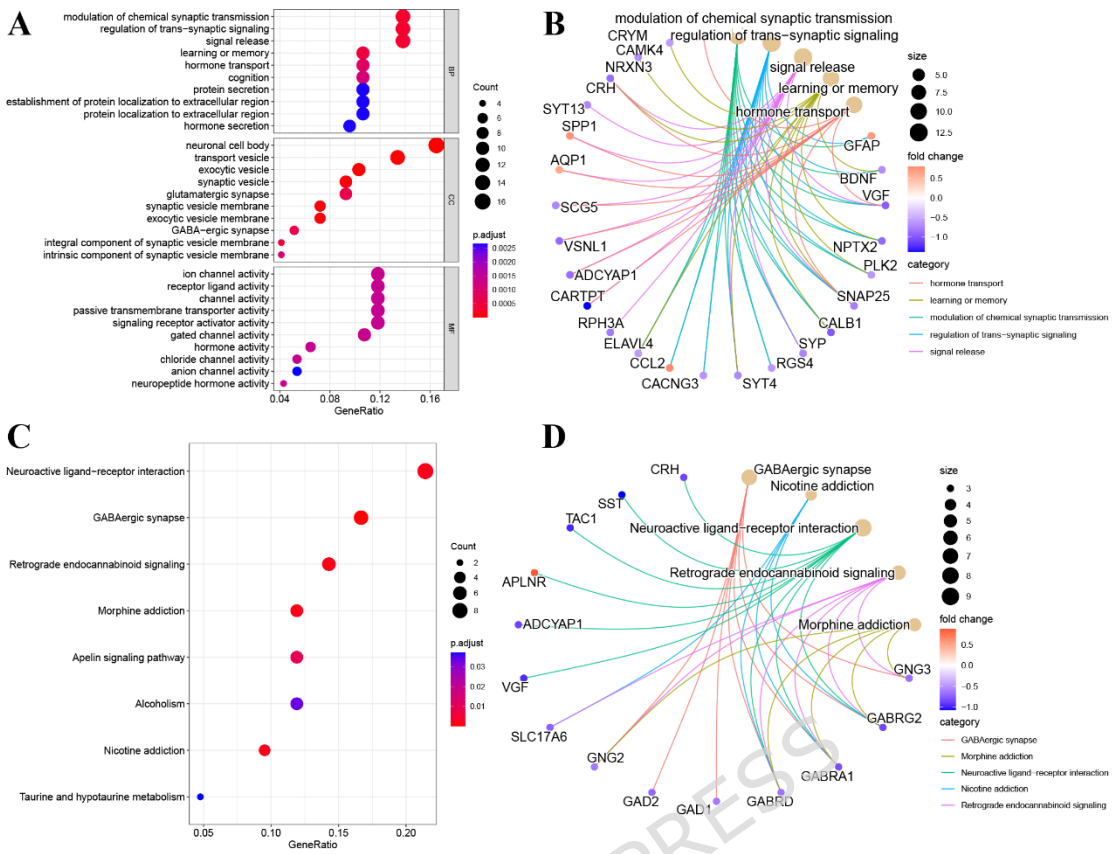

Fig. 3 Biofunctional enrichment analysis of DEGs. **(A-B)** GO functional enrichment analyses of DEGs highlighting the top 10 terms in biological process (BP), cellular component (CC), and molecular function (MF) categories. The results of GO were presented by bar plot and circle charts. **(C-D)** KEGG pathway analysis of the intersection of DEGs. KEGG results were presented using bubble and circle graphs.

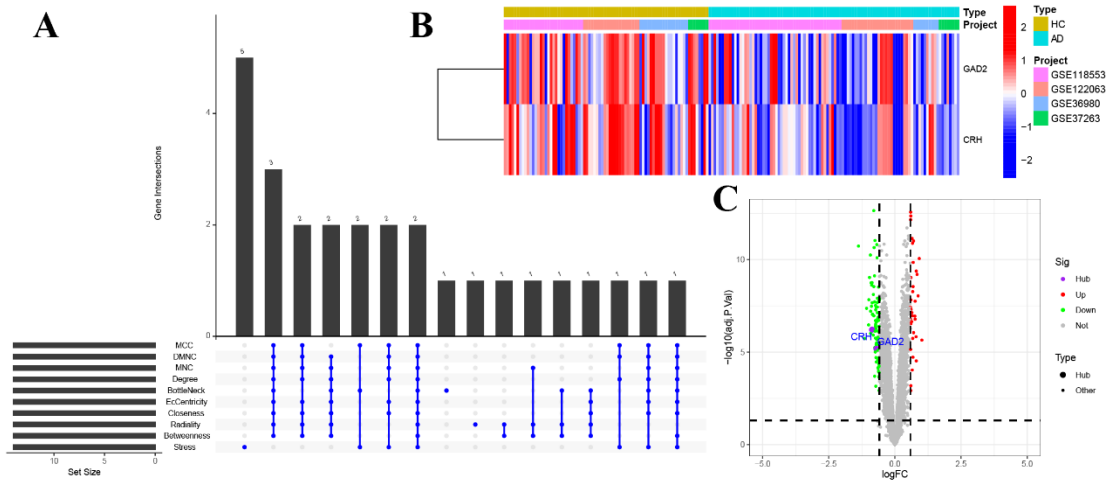

Fig. 4 Identification of hub Genes. **(A)** The R package 'UpSet' was utilized to screen hub genes using ten different algorithms. **(B)** A heatmap illustrating the expression of two hub genes was generated using the combined microarray data. Columns represent the hub genes CRH and GAD2, rows represent individual samples. The color scale indicates the normalized expression level (log2 scale) of each gene, with red indicating higher expression and blue indicating lower expression. **(C)** Volcanic plot was used to depict the ultimate DEGs and hub genes.

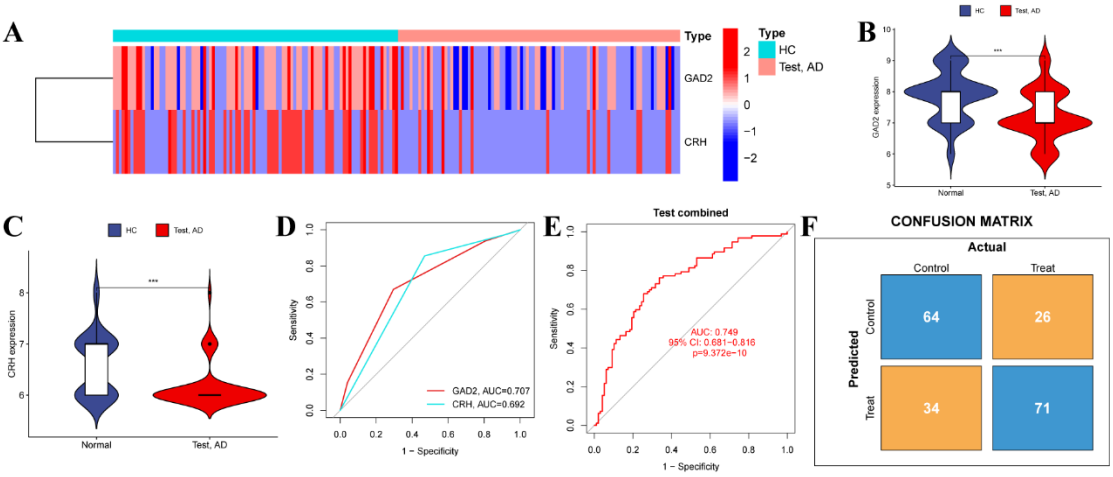

Fig. 5 Validation of hub genes through external sources. **(A)** A heat map illustrating the transcriptional profiles of hub genes in the validation dataset GSE132903. Columns represent the hub genes CRH and GAD2, rows represent samples from the GSE132903 dataset (AD vs. HC). The color scale indicates the relative expression level (normalized counts, log2 scale), with red indicating high expression and blue indicating low expression. **(B-C)** Box plots illustrating hub gene expression in the GSE132903 validation dataset. **(D)** ROC curves for hub genes in the validation dataset GSE132903. **(E)** The ROC curve displays the combined two biomarkers' diagnostic accuracy AUC > 0.7 suggested that the model's effect was well-fitting. **(F)** Confusion matrix for validation set. ROC stands for receiver operator characteristic, and AUC refers to the area under the curve. ***$p < 0.001$.

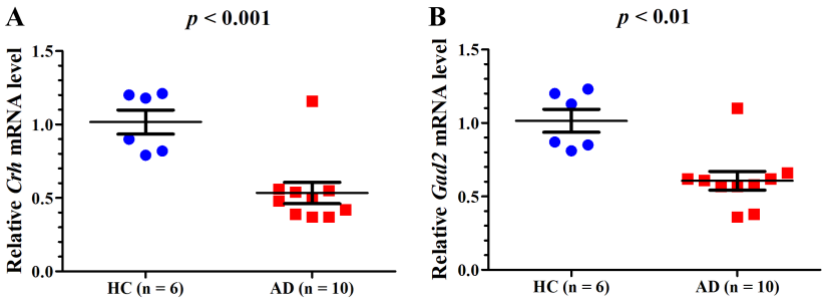

Fig. 6 RT-qPCR was used to analyze the relative expression levels of hub genes in the temporal cortex of AD patients compared to healthy controls. Panel **(A)** shows the relative mRNA expression of CRH, and Panel **(B)** displays that of GAD2.

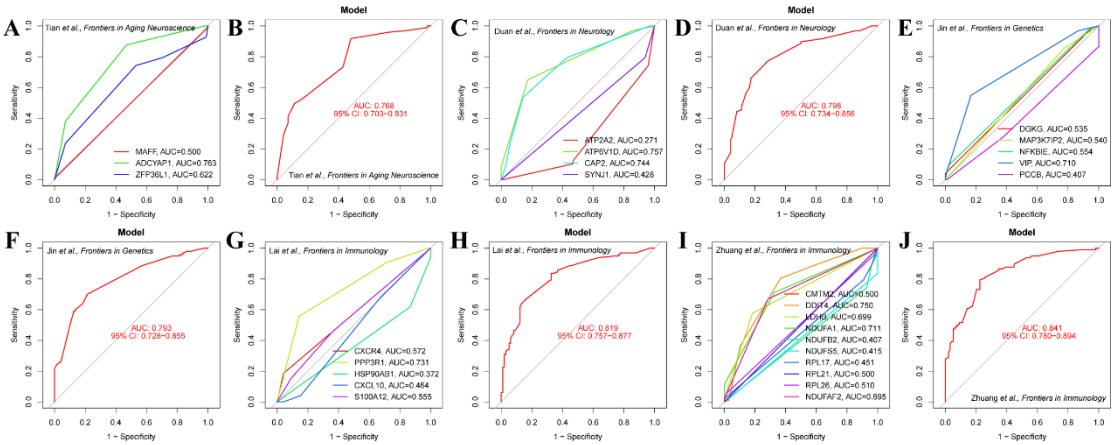

Fig. 7 Our diagnostic biomarkers were compared to published biomarkers to externally validate their diagnostic effectiveness. **(A, C, E, G, and I)** The diagnostic effectiveness of published AD biomarkers was validated using ROC analysis on the GSE132903 dataset. **(B, D, F, H, and J)** Confusion matrix for published biomarkers was validated by validation set.

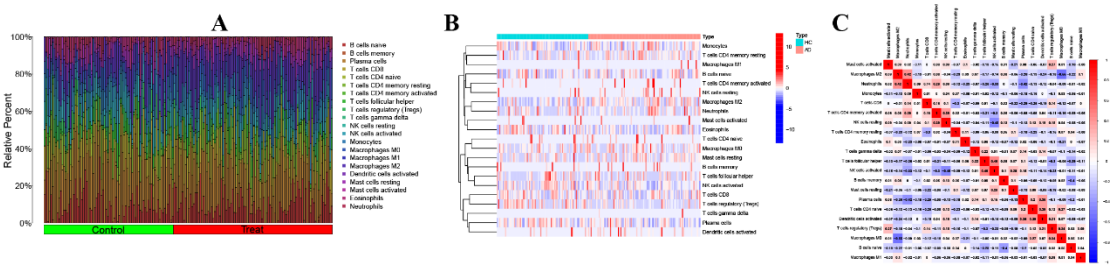

Fig. 8 Immune cell infiltration in AD and control samples. A histogram **(A)** and a heatmap **(B)** depicted the composition of 22 immune cell types in each sample. In panel (B), columns represent the 22 immune cell types, and rows represent individual samples. The color scale (see legend) indicates the relative proportion of each immune cell type (CIBERSORT fraction) within a sample, ranging from low (blue) to high (red). **(C)** The study assessed the correlation among 22 immune cell types in AD. Red indicates a positive correlation, while blue signifies a negative correlation. The color intensity represent the magnitude of the Spearman correlation coefficient.

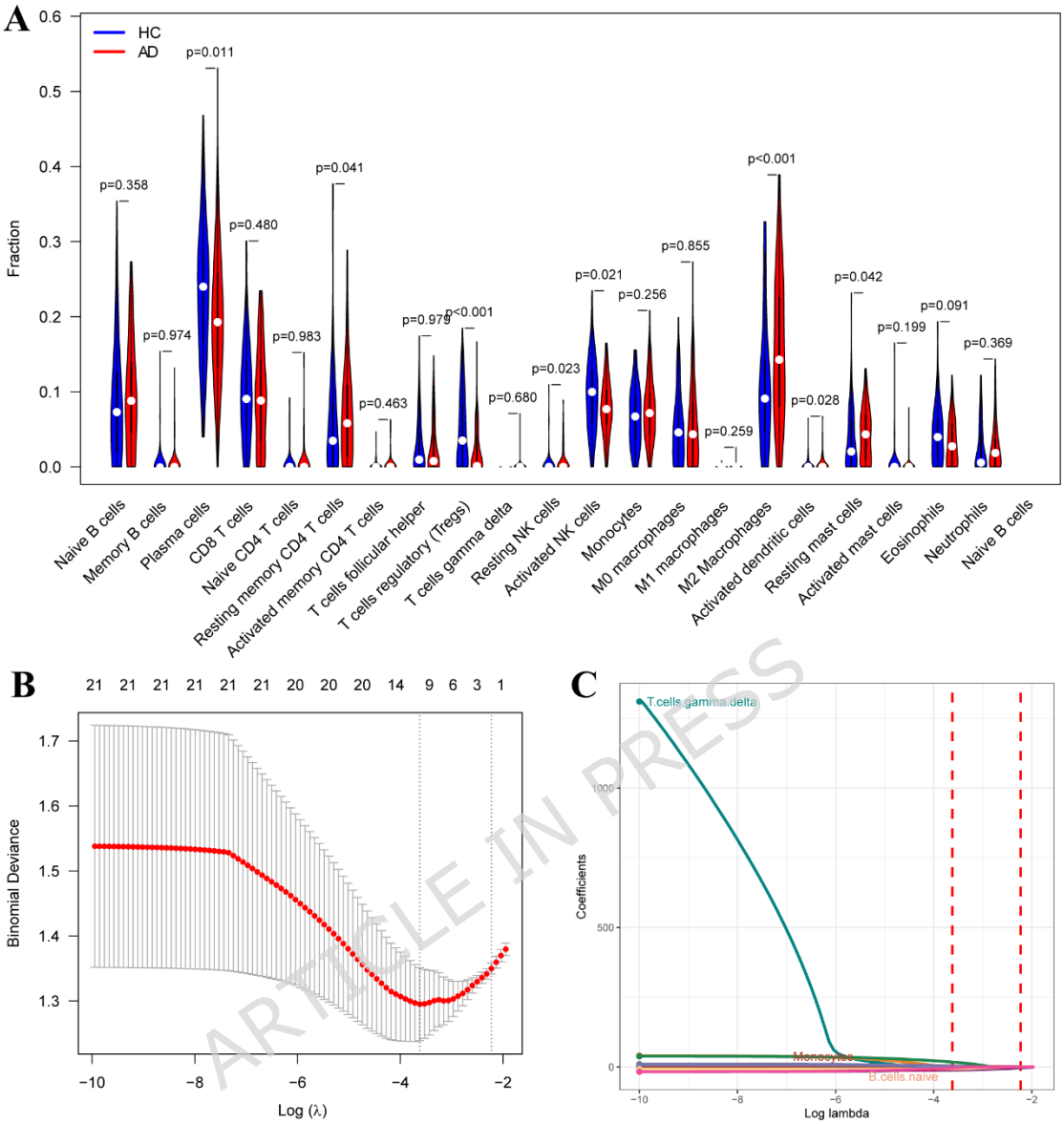

Fig. 9 Analyzing distinct immune cell infiltrates in AD. **(A)** The violin plot illustrates the variation in immune cell infiltration between AD and control samples. **(B-C)** LASSO regression was performed to examine the varying immune cell infiltrates between AD and control samples. The vertical dashed line indicates the lambda.1se value used for selecting the final model.

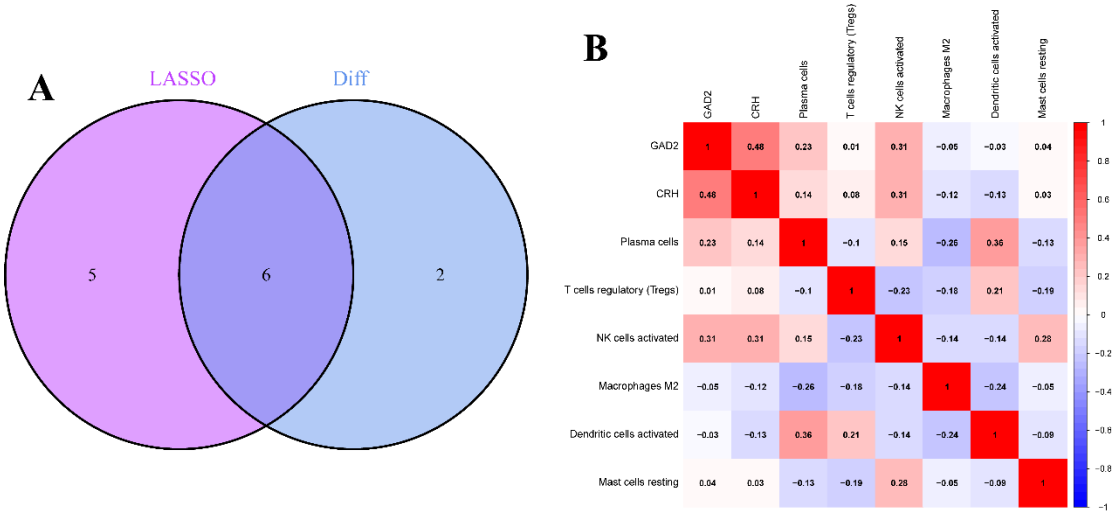

Fig. 10 Correlation analysis between biomarkers and distinct immune cell populations in AD. **(A)** A Venn diagram was used to identify the intersection of differential immune cells identified by both the Wilcoxon test and LASSO regression methods. **(B)** Correlation among two effective biomarkers and 6 significantly differential immune cells.

Table 1. Datasets from GEO employed in this study

GEO	Type	Platform	Tissue (Homo sapiens)	Sample size			Mean Age ± SD (Range)	Sex (Male/Female)
				Total	HC	AD		
GSE36980	mRNA	GPL6244	Temporal cortex	29	19	10	HC: 76.7 ± 10.1 (54-89) AD: 89.8 ± 4.3 (83-95)	HC: 8 Male / 11 Female AD: 5 Male / 5 Female
GSE37263	mRNA	GPL5175	Temporal cortex	16	8	8	HC: 80.1 ± 7.1 (66-87) AD: 72.6 ± 9.1 (63-88)	HC: 5 Male / 3 Female AD: 5 Male / 3 Female
GSE118553	mRNA	GPL10558	Temporal cortex	83	31	52	HC: 69.2 ± 16.8 (40-95) AD: 82.4 ± 10.7 (63-105)	HC: 19 Male / 12 Female AD: 23 Male / 29 Female
GSE122063	mRNA	GPL16699	Temporal cortex	50	22	28	HC: 78.8 ± 8.6 (60-91) AD: 81.0 ± 6.7 (63-91)	HC: 10 Male / 12 Female AD: 6 Male / 22 Female
GSE132903	mRNA	GPL10558	Middle temporal gyrus	195	98	97	HC: 85.0 ± 6.9 (70-102) AD: 85.0 ± 6.7 (70-98)	HC: 50 Male / 48 Female AD: 49 Male / 48 Female

Table 2 List of primers for RT-qPCR

Primer	**Sequence (5′→ 3′)**
CRH-F	AGGCACCGGAGAGAGAAAGG
CRH-R	TTGCTGTGCTAACTGCTCGG
GAD2-F	CGGGTTTGAAGCGCATGTTG
GAD2-R	GTGTGCTGAGGCTTCCCATC
GAPDH-F	ATGGCAAATTCCATGGCACC
GAPDH-R	GACTCCACGACGTACTCAGC